Full-Bandwidth Mission Profile Emulation of the Electric Machine System With Voltage Reference Signal Transmission

Yuhao Qi, *Student Member, IEEE*, Ke Ma, *Senior Member, IEEE*, and Weiyu Tang

***Abstract*—Electric machine emulation (EME) is becoming a popular solution in advanced testing and validation of power-electronics-based machine drive systems. In terms of a typical EME, the stator current references are first calculated in response to the sampled terminal voltage, and then, are electrically generated by power electronics converters. In this type of structure, closed-loop current control and low-pass sampling for the voltage are inevitably introduced, resulting in distortion in frequency-domain behaviors of EME. Consequently, the steady-state performance under a high fundamental frequency, and the dynamic performance under load transients, may deviate from those of the target machine system. In this article, the bandwidth limitations of the typical EME are identified and analyzed in detail, and a novel structure that realizes full-bandwidth mission profile emulation is proposed. Theoretical analyses are given to prove that the frequency-domain characteristics of the proposed structure would be identical to the actual machine systems, which allows for the extended operating range of mission profile emulation. Simulation and experimental results are provided to validate the effectiveness of the proposed method.**

***Index Terms*—Control structure, electric machine emulation (EME), frequency-domain analysis, mission profile, reliability, testing.**

I. Introduction

NOWADAYS, relatively high-speed electric machines (HSEMs) with fast control dynamics have been widely used in various important applications, such as electric vehicles/transportations, aerospace, and high-precision industry processing. In these applications, stringent requirements for reliability of overall systems make it crucial to validate the control functions as well as the reliability performances of the power electronics system before they are put into real-filed operation.

Manuscript received January 19, 2021; revised May 18, 2021 and August 5, 2021; accepted August 28, 2021. Date of publication September 3, 2021; date of current version November 30, 2021. This work was supported in part by the National Nature Science Foundation of China through Project 51777123 and in part by the Power Electronics Science and Education Development Program of Delta Group. Recommended for publication by Associate Editor J. Ye. (*Corresponding author: Ke Ma.*)

The authors are with the Key Laboratory of Control of Power Transmission and Conversion, Ministry of Education, Shanghai Jiao Tong University, Shanghai 200240, China, and also with the Department of Electrical Engineering, Shanghai Jiao Tong University, Shanghai 200240, China (e-mail: qiyuhao0@sjtu.edu.cn; kema@sjtu.edu.cn; longjinpeter@alumni.sjtu.edu.cn).

Color versions of one or more figures in this article are available at https://doi.org/10.1109/TPEL.2021.3109877.

Digital Object Identifier 10.1109/TPEL.2021.3109877

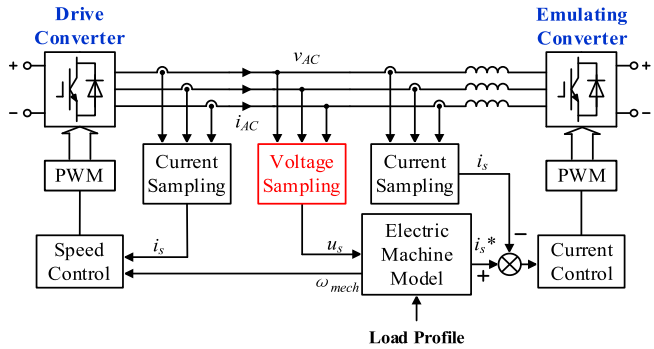

Fig. 1. Typical configuration of the EME system.

[1]–[6]. The typical testing method for the machine drive normally includes extra motors and mechanical parts to recreate the required loads for the system under test [7]. However, there are several disadvantages for this mechanical-based testing solution, which are as follows:

1) bulky, expensive, and inapplicable for long-term operation;
2) limits in dynamic to emulate complex mission profiles;
3) poor efficiency and safety.

Consequently, more advanced, flexible, and efficient testing techniques are becoming emerging needs.

Given aforementioned problems, electric machine emulations (EMEs) are proposed, which are originally named as virtual machines [8]. EMEs can generally be divided into three groups: controller hardware-in-the-loop simulations (CHILS), power hardware-in-the-loop simulations (PHILSs), and power-electronics-based emulations (PEBEs), which have different characteristics and suitable testing scenarios. Efforts have been put on the implementation of EMEs targeting various kinds of electric machines, e.g., the induction motors in [9]–[11], the virtual synchronous generators (VSGs) in [12]–[14], and the permanent-magnet synchronous machines (PMSMs) in [15]–[20]. These typical EMEs can perform well in a low rotational speed and steady state, with the generalized configuration summarized in Fig. 1. However, when it comes to a higher rotational speed and fast dynamics, the performances of these emulation approaches are not satisfactory. In fact, the low-pass filter (LPF) for voltage sampling and the closed-loop current control (CLCC)

is highly correlated to the distortion in the high-frequency static and dynamic performance of the EME.

In terms of the LPF for voltage sampling, in [15] and [16], a pulsewidth modulation (PWM) stator voltage sampling method is applied by increasing the sampling frequency significantly. The sampling frequency is set to be about 16–20 times of the switching frequency in the drive-side converter. Thus, the PWM stator voltage information can be sampled with less distortion. However, the overenhancement of the sampling frequency imposes a high cost and demand for the digital processor in the emulating-side converter, because some complex control functions should be reserved and the control frequency could not be synchronized with the high sampling frequency. In [17], a PWM stator voltage sampling method with the help of a comparator is used. The rising and falling edges of the PWM voltage from the drive-side converter can be detected, and the stator voltage and current response of the target machine is calculated by the embedded iteration model. However, the EME system always needs to reserve certain computational resources for the control strategy and model calculation. The voltage sampling method based on the comparator and the subsequent iterative model calculation may overoccupy the computational resource, which may also result in extra system computation delay.

In terms of the CLCC, in [18], the bandwidth of the CLCC in EME is enhanced to alleviate its influence on the drive-side converter. However, it is quite difficult to adjust the bandwidth of the current loop of EME, because the drive side is typically viewed as a black box during tests, and the control parameters are difficult to be accurately acquired. At the same time, overenhanced proportional–integral (PI) parameters will cause the instability of the whole drive and emulation system. Lee *et al.* [16] and Luo *et al.* [17] try to increase the CLCC equivalent bandwidth with the help of silicon carbide (SiC)-based MOSFET through a higher switching frequency. However, this approach may have limited application with respect to the power level and results in a high cost. Paralleled or interleaved converters are adopted in [21] and [22] to achieve a higher equivalent switching frequency, but the current sharing problems between multiple converters need to be further discussed, and the cost will linearly increase with the number of the paralleled or interleaved converters. Amitkumar *et al.* [23] uses a linear amplifier as the emulating power stage, and the bandwidth of linear amplifiers can reach dozens of kilohertz. However, linear amplifiers are not suitable for high-power scenarios, and other drawbacks, such as high costs, high weight, and low efficiency, restrict the use of linear amplifiers in the application of long-term tests. In [11] and [17], a model-predictive-control controller is employed instead of the CLCC to extend the emulation bandwidth, which will definitely increase the computational resources of the emulation side, and the stability cannot be guaranteed as the mission profile and fundamental frequency varies.

For HSEM systems, typical EME approaches are not applicable due to their limited performance in emulating the complete characteristic of the actual system. As a result, the EME system will lose stability or have a poor tracking ability when load steps or sudden speed changes occur in the mission profile. Furthermore, there is still a lack of effort focusing on the modeling and analysis of bandwidth for mission profile emulation in the existing work. A kind of low-cost and high-efficiency EME is in urgent need.

In this article, the limitations of the typical method based on the LPF for the voltage sampling and the CLCC are analyzed. A novel method is proposed to realize an emulation of the full-bandwidth mission profile, and the frequency-domain characteristics of this method would be theoretically identical to an actual electric machine. The proposed EME is based on the PEBE. Different from PHILS, the proposed EME gets rid of the expensive real-time simulator and can be controlled flexibly. The detailed modeling along with the control design for this approach is also implemented. The feasibility of the proposed method is validated by simulations and prototypes. Compared with the existing methods, superiorities can be summarized as follows.

1) The LPF for voltage sampling is replaced by the voltage reference signal transmission. The hardware and computational costs are reduced, and the emulation accuracy as well as control bandwidth are improved, and the frequency range of the mission profile can be significantly extended.
2) The CLCC in the emulating side is replaced with the open-loop current control (OLCC), decoupling certain interactions between the drive-side controller and the emulating-side controller, reserving the current control characteristics from the drive-side controller, to achieve better robustness, lower computational resources, and higher control bandwidth.
3) The combination of the voltage reference signal transmission and the OLCC can further help to eliminate the delay of PWM modulations. Thereby, the proposed EME can realize an emulation in the full bandwidth, compared with the emulated electric machine drive system. Stability and followability can be guaranteed, especially for mission profiles with a relatively high frequency and fast dynamics.

II. Bandwidth Limitation of the Typical Approach to Achieve EME

The PMSM is chosen as the study case in this article, for it is widely used in modern electric drive system and is a suitable candidate for high-speed applications. The critical parameters of the studied PMSM for analysis are summarized in Table I. The drive-side converter is operated with most typically used field-oriented control (FOC). The typical configuration of the EME system can be summarized in Fig. 1, which consists of the drive-side converter and the emulating-side converter, and the two converters are connected by the interface filter inductance.

The drive-side converter is set to work in a voltage-source-converter (VSC) mode. Under this premise, the stator current of the target PMSM is the response to the stator voltage. This feature can also be concluded from the equivalent control diagram, as shown in Fig. 2. By ignoring the hysteresis, asymmetry, and other disturbance, the transfer function of the stator current response of the target PMSM can be simplified as the stator

TABLE I
PARAMETERS OF THE PMSM-DRIVE SYSTEM FOR BENCHMARKING THE SIMULATION

Variable	Symbol	Value	Unit
Stator Inductance(d-axis)	L_d	0.12563	mH
Stator Inductance(d-axis)	L_q	0.12563	mH
Stator Resistance	R_s	0.01385	Ω
PM Flux Linkage	ψ_f	0.03859	Wb
Number of Pole Pairs	N_p	2	-
Rotational Inertia	J	0.003	kg·m^2
Friction Coefficient	F	0	kg·m^2/s
Inductance of *LCR*	Lf	0.2	mH
Capacitor of *LCR*	Cf	30	uF
Resistor of *LCR*	Rf	3	Ω
DC Bus Voltage	V_{DC}	400	V
Switching Frequency	f_{sw}	20	kHz

admittance [24]–[26]

$$G_{\mathrm{Stator}}(s) = \frac{1}{sL_S + R_s} \tag{1}$$

where L_s and R_s are the equivalent inductance and resistance of the PMSM stator, respectively, and s is the differentiator. It is worth to mention that more accurate mathematical models of the electric machine can be applied [27], [28], such as time-variant electric machine models and the finite-element-method models, but this topic has been well analyzed and is not the focus of this article.

The control diagram of the typical EME is plotted in Fig. 2, as well as the one based on the target PMSM for emulation. It can be seen clearly that, compared to the target PMSM, there are two extra parts in EME at the input and output of the transfer function for the electric machine admittance $G_{\mathrm{Stator}}(s)$.

For the first part, a voltage sampling and filtering stage has to be added at the input of $G_{\mathrm{Stator}}(s)$ because the voltage generated by the drive-side converter is PWM waveforms, which cannot be directly sensed by the digital processor. It is assumed that an *LCR* filter is utilized as the LPF for the voltage sampling in this article. The transfer function of the LPF for voltage sampling is modeled as

$$G_{\mathrm{sampling}}(s) = \frac{1}{s^2 L_{\mathrm{sam}} C_{\mathrm{sam}} + sR_{\mathrm{sam}} + 1} \tag{2}$$

where L_{sam}, R_{sam}, and C_{sam} are the inductance, resistance, and capacitance of the *LCR* sampling filter for the PWM voltage, respectively.

For the second part, the CLCC is used at the output of $G_{\mathrm{Stator}}(s)$ to regenerate the current to emulate the response of an actual machine. A current filter and a PI controller are used in this article. The open-loop transfer function of the CLCC is expressed as (3), and the closed-loop transfer function can be expressed as $G_{\mathrm{current\_close'}}(s)$

$$G_{\mathrm{current\_open'}}(s) = e^{-sT}\frac{sK_{pi'} + K_{ii'}}{s^2 L_f + sR_f} \tag{3}$$

where K_{pi}' and K_{ii}' are the PI parameters of the closed-loop control, L_f and R_f are the inductance and resistance of the current filter, respectively, and T is the control time.

Consequently, the equivalent stator admittance $G_{\mathrm{Stator'}}(s)$ based on the EME is built, which is expressed as (4). As can be seen, it is the two extra parts $G_{\mathrm{sampling}}(s)$ and $G_{\mathrm{current\_close'}}(s)$ that cause distortion in the mission profile emulation. The filter for the voltage sampling can be seen as a second-order LPF, whereas the CLCC can be seen as a first-order LPF.

$$G_{\mathrm{Stator'}}(s) = G_{\mathrm{Stator}}(s) \cdot G_{\mathrm{sampling}}(s) \cdot G_{\mathrm{current\_close'}}(s). \tag{4}$$

The Bode diagram of the inner current loop (from $I*$ to I_{stator}) of FOC based on typical EME is plotted and is compared with that on the actual PMSM, as illustrated in Fig. 3. In order to cover a wide range of the analysis, two kinds of PMSMs are chosen as the study case in this article. The parameters of the target PMSMs under emulation is listed in Tables I and II. The resonant frequency of the *LCR* LPF for voltage sampling is set to one-fourth of the switching frequency, and the bandwidth of the CLCC in EME is designed around 5% of the switching frequency of the emulating converter.

The Bode diagram of the current control loop based on the typical EME and the target PMSM can be divided into three regions in the frequency bands, as can be seen in Fig. 3. In region I, where the frequency range is below 5% of the switching frequency, the magnitude-frequency responses of the two systems are almost the same. In region II, where the frequency range is between 5% and 25% of the switching frequency, there are about –20 dB/decade difference in the magnitude response, and about 180° difference in the phase angle. The differences under frequency domain are mainly caused by the extra current control loop in EME. In region III, where the frequency range is above 25% of the switching frequency, the LPF for voltage sampling overenhances the attenuation slope difference to –60 dB/decade. What is more, the three distortion zones have not changed as the target machine and FOC parameters change, which completely depend on the CLCC and LPF for voltage sampling.

According to the Bode diagram, it can be concluded that there are two major aspects of the limitations for the performance of the typical EME method, which are as follows.

1) The difference in frequency band regions II and III will distort the dynamic performances. In case the operation condition changes, like the load steps or the stator starts to accelerate or decelerate, the control behaviors of the drive side will greatly change.
2) When the target electric machine is working at a relatively high speed, the stability of the complete FOC system will be adverse due to the distortion in frequency bands II and III.

III. PROPOSED EME CONFIGURATION TO IMPROVE THE BANDWIDTH LIMITATIONS

Considering that the LPF for voltage sampling and extra current control loop will cause behaviors distortion in medium- and high-frequency band, the main idea is to eliminate these two elements by manipulating the structure.

First, the LPF for voltage sampling can be avoided. There are commonly three methods to capture the PWM-shape voltage without using an LPF, which are as follows.

1) Increase the sampling frequency over higher than the switching frequency [15], [16].

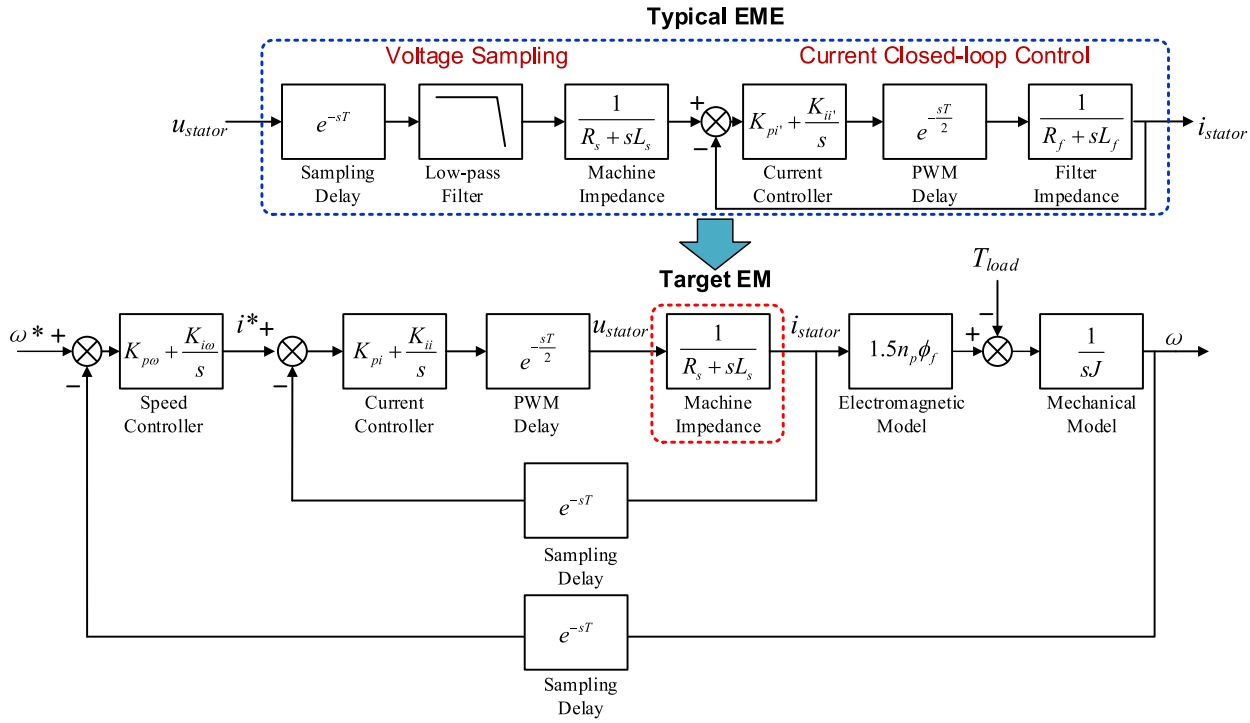

Fig. 2. Control diagram of the FOC loop for a typical PMSM system and the typical EME.

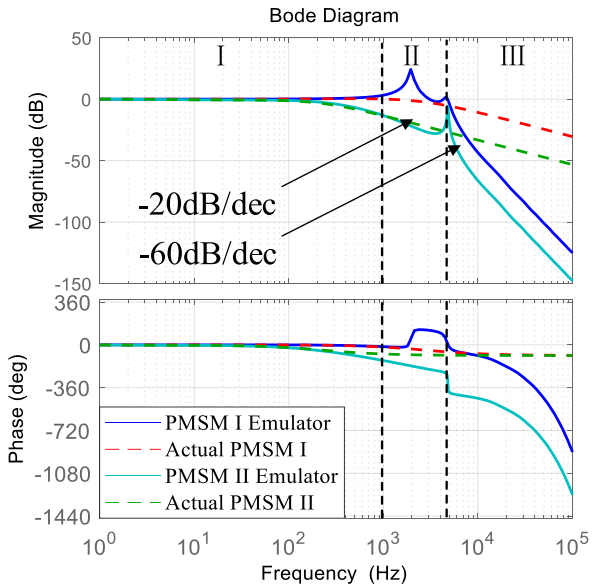

Fig. 3. Bode diagram of the current inner loop in FOC based on the typical EME and the actual PMSMs.

2) Use a comparator in the circuit to detect the rising and falling edges of the PWM voltage [17].
3) Directly transmit the linear modulation references from the drive side to the EME.

For the DSP-based EME, the overenhancement of the sampling frequency imposes high cost and demand for the digital processor, whereas the use of the comparator needs more complex iteration model and may overoccupy the computational resource. In this article, the transmission of the linear modulation reference signal from the drive to EME is used, thus most of the distortion caused by the low-pass sampling filter can be eliminated.

Second, the CLCC can be avoided as well. The OLCC is a more suitable choice in this case, which is equivalent to an all-pass filter. The OLCC normally can achieve better dynamic performances, and there will be no static and dynamic error under the FOC control mode. The accuracy of the OLCC can be improved by more accurate modeling of the interface filter and the target machine.

Moreover, it should be noted that in the EME and drive system, the stator current is not only controlled by the OLCC in the emulating side, but also controlled by the inner CLCC and speed control loop in FOC in the drive side. These loops will help realize the current and voltage control, such as the noise and harmonics suppression, dead-time and conducting voltage compensation, and so on, which is on their own duty.

TABLE II
PARAMETERS OF THE PMSM-DRIVE SYSTEM FOR BENCHMARKING THE EXPERIMENT

Variable	Symbol	Value	Unit
Stator Inductance(d-axis)	L_d	2.5	mH
Stator Inductance(d-axis)	L_q	2.5	mH
Stator Resistance	R_s	0.34	Ω
PM Flux Linkage	ψ_f	0.022	Wb
Number of Pole Pairs	N_p	4	-
Rotational Inertia	J	0.002	kg·m^2
Friction Coefficient	F	0	kg·m^2/s
DC Bus Voltage	V_{DC}	400	V
Switching Frequency	f_{sw}	20	kHz

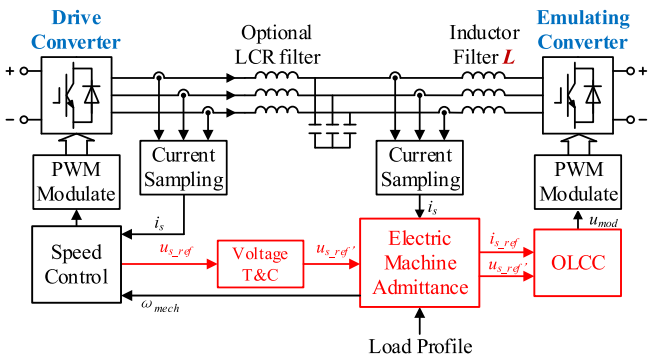

Fig. 4. Flowchart of the EME realizing the full-bandwidth mission profile emulation.

In some high-speed mission profiles for emulation, the *dq* inductance of the HSEM is normally designed to be relatively low in order to achieve a higher fundamental frequency with limited the dc supply voltage, this will result in large current ripple and harmonics in the machine drive system and put challenges for EME. One method adopted extensively to solve this problem is by using the *LCR* filter [29]. When the *LCR* or other passive filters are used in the drive system, the voltage reference signal transmitted to the emulating side of EME should be corrected through compensating the voltage drop on the filter.

Consequently, a voltage correction part, which can enhance the accuracy of the mission profile emulation and control behaviors reconstruction, is introduced. The overall EME structure realizing the full-bandwidth mission profile emulation is constructed in Fig. 4. The linear voltage reference signal u_{s_ref} on the drive side is directly transmitted to the emulating converter through a voltage transmission and correction part. The modulation voltage u_{mod} is generated through the electric machine admittance model and OLCC.

It should be noted that because the drive side can be seen as a black box and its control behavior is unknown, the design of the speed PI controller and the current PI controller depends on the converter under test, and do not need to be covered by the proposed EME. This is an advantage achieving decoupling between the tested drive side and the emulating side. Thus, the proposed EME can be plug-and-play for higher robustness.

IV. Modeling and Control of the Proposed EME Method

In contrast with the typical EME, the control methods of the proposed structure are significantly different. It mainly contains two parts as shown in Fig. 4: the calculation of reference current i_{s_ref} based on the electric machine admittance and the calculation of the EMEs modulation voltage u_{mod} based on the OLCC. For simplicity of analysis, the control delay and modulation delay are ignored at first during the modeling and design process, and the influence of the delay on the whole emulation system will be discussed in the end of this session.

First, the reference current i_{s_ref} can be calculated according to the frequency-domain model of the PMSM [24]–[26]. Under frequency domain, the *d*- and *q*-axes components of the terminal voltage of the PMSM are expressed as (5) so that the electric machine reference current i_{s_ref} can be calculated from the voltage modulation signal u_{s_ref} in the drive side by the admittance model (6)

$$\begin{aligned} u_d &= i_d(sL_d + R_s) - \omega_e L_q i_q \\ u_q &= i_q(sL_q + R_s) + \omega_e L_d i_d + \omega_e \psi_f \end{aligned} \tag{5}$$

$$\begin{aligned} i_{sd\_\mathrm{ref}} &= \frac{u_{sd\_\mathrm{ref}} + \omega_e L_q i_{sq\_\mathrm{ref}}}{sL_d + R_s} \\ i_{sq\_\mathrm{cmd}} &= \frac{u_{sq\_\mathrm{ref}} - \omega_e L_d i_{sd\_\mathrm{ref}} - \omega_e \psi_f}{sL_q + R_s}. \end{aligned} \tag{6}$$

On the other hand, the modulation voltage u_{mod} of the emulating converter can be calculated based on the OLCC. If the interface filter is an inductance, the u_{mod} can be calculated by (7), according to its mathematical model

$$\begin{aligned} u_{d\_\mathrm{mod}} &= u_{sd\_\mathrm{ref}} - i_{sd\_\mathrm{ref}}(sL_f + R_f) + \omega_e L_f i_{sq\_\mathrm{ref}} \\ u_{q\_\mathrm{mod}} &= u_{sq\_\mathrm{ref}} - i_{sq\_\mathrm{ref}}(sL_f + R_f) - \omega_e L_f i_{sd\_\mathrm{ref}}. \end{aligned} \tag{7}$$

However, the direct use of (7) to calculate the emulating converter's modulation voltage u_{mod} will introduce the differentiator operation, which is sensitive to signal noises and will cause magnitude–frequency distortion. By combining (6) and (7), a new function (8) can be obtained. At this time, the differentiator introduced by the electric machine impedance is compensated by the interface filter *L* of the emulating converter.

$$\begin{aligned} u_{od} &= (u_{sd\_\mathrm{ref}} + \omega_e L_q i_{sq\_\mathrm{ref}}) \frac{sL_d + R_s}{sL_f + R_f} \\ &\quad + (u_{sd\_\mathrm{ref}} + \omega_e L_f i_{sq\_\mathrm{ref}}) \\ u_{oq} &= (u_{sq\_\mathrm{ref}} - \omega_e L_q i_{sd\_\mathrm{ref}} - \omega_e \psi_f) \frac{sL_q + R_s}{sL_f + R_f} \\ &\quad + (u_{sq\_\mathrm{ref}} - \omega_e L_f i_{sd\_\mathrm{ref}}). \end{aligned} \tag{8}$$

The complete signal flow to derive the modulation signal of the emulating-side converter is constructed in Fig. 5, which can be divided into two parts. Part I is the calculation of the reference current i_{s_ref} according to the electric machine admittance. And Part II is the calculation of modulation voltage based on (8) according to the signal flow of the OLCC. There is no closed-loop controller or iteration calculation, and the use of the differentiator in the model of filter impedance can be avoided. Thus, the stability can be guaranteed and no suffering from the sampling noise or phase lag will occur.

Moreover, the torque model and mechanical model are also constructed as follows:

$$T_e = \frac{3}{2} p_n(\psi_f i_q + (L_d - L_q) i_d i_q) \tag{9}$$

$$T_e - T_L = J\frac{d\omega}{dt} + F\omega. \tag{10}$$

In case of the high-speed mission profile, if an *LCR* filter is used in the target machine drive system to suppress the ripple current, a voltage correction part is applied to the EME system, as illustrated in Fig. 6. The output of the voltage correction part u_{s_ref}' acts as the updated input signal of Part I in Fig. 5 so that

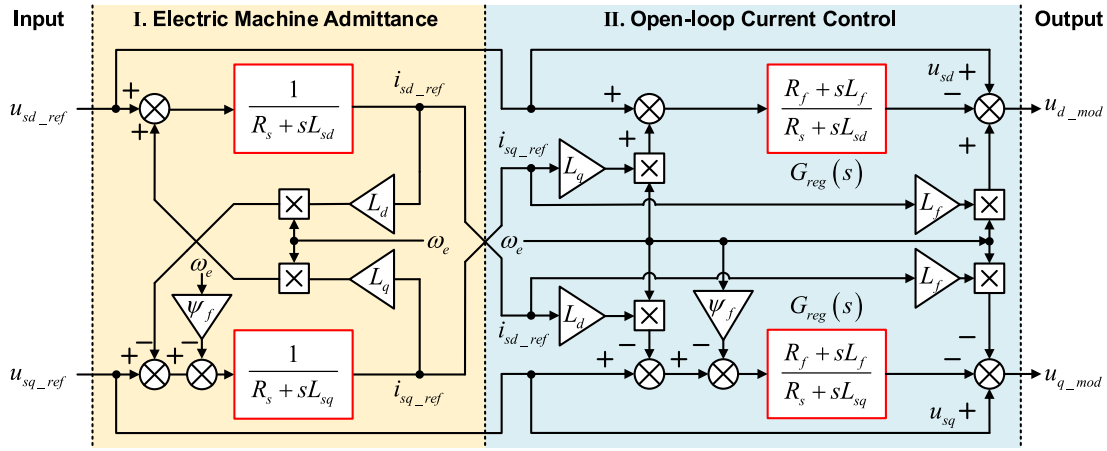

Fig. 5 Signal flow of the EME realizing full bandwidth in the *dq* frame. u_{s_ref}—The input signal of the electric machine admittance model; and u_{mod}—The output signal of the OLCC.

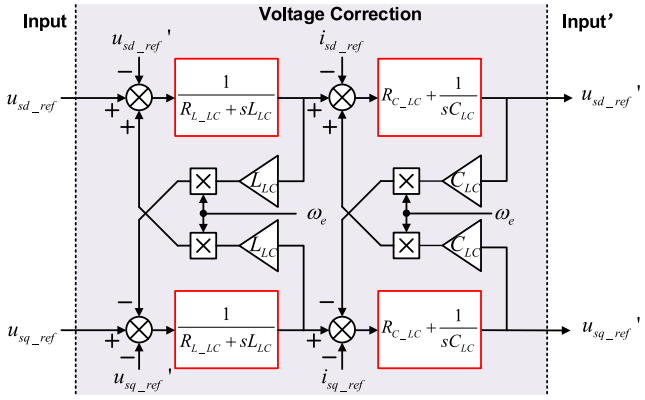

Fig. 6. Signal flow of the voltage correction in the *dq* frame. u_{s_ref}—The input signal of the voltage correction; u_{s_ref}'—The output signal of the voltage correction and the updated input of the electric machine admittance.

the voltage drop on the *LCR* filter can be compensated and more accurate emulating results can be achieved. Moreover, there is no direct use of the differentiator. So that there will be little distortion caused by the direct use of the differentiator in any discretization methods (like Tustin method or Backward Euler method).

The complete control diagram of EME realizing the full-bandwidth mission profile emulation is illustrated in Fig. 7. In contrast to the typical approach, the proposed EME replaces the LPF for voltage sampling with the voltage transmission and compensation, and replaces the CLCC with the OLCC.

As shown in Fig. 7, by using the voltage reference signal transmission and OLCC together in the proposed EME, which realizes the full-bandwidth emulation, the distortion caused by extra PWM modulation delay in the emulating side can also be compensated, as illustrated in Fig. 2. When the DSPs are working in the synchronous mode, the PWM delay in the OLCC can be compensated by the PWM delay link in FOC. Better stability and high bandwidth can be guaranteed. Thus, the voltage reference signal transmission and OLCC working together can take more significant effects than themselves.

According to the modeling and analysis, the Bode diagram of the current loop in FOC based on EME, and that based on the target PMSMs for emulation, are illustrated in Fig. 8. Compared with the bode diagram of the typical EME in Fig. 3, a significant improvement in the emulation of the middle and high-frequency band of target PMSMs can be achieved. The proposed EME method can realize full-bandwidth emulation theoretically so that a very accurate emulation performance can be achieved.

V. Simulation and Experiment Validation

A. *Simulation Validation—Steady-State Performance in a High-Speed Machine*

To verify the feasibility of the method proposed in this article and make a comparison with the typical ones, the simulations are made based on PLECS. The topology and emulation strategy are consistent with Figs. 1 and 4. The target electric machine parameters are listed in Table I, which is chosen as an HSPMSM and an *LCR* filter used.

Various official mission profile standards have been introduced in actual electric vehicle testing, such as extra urban driving cycle (EUDC), the federal test procedure (FTP-75), Japanese 10-15, and so on. These relatively gentle mission profiles always introduce a long testing time scale, which is longer than half an hour. And the purpose of using these mission profiles is to test certain functions of the devices in the electric vehicles (EVs) (such as the batteries capacity and control functions). However, in order to verify the emulation bandwidth and the characteristics in the high-frequency band of the EMEs, these basic function tests are not concerned. The mission profile study case should be designed to be more severe under short-time scales to cover a wide frequency band. Thus, the dynamic and static performance of the EMEs under short-time scales is to be focused and emphasized.

In order to meet the requirements for testing the dynamic and static performance under short-time scales, the mission profile study case selected in this article is designed according to the following criteria.

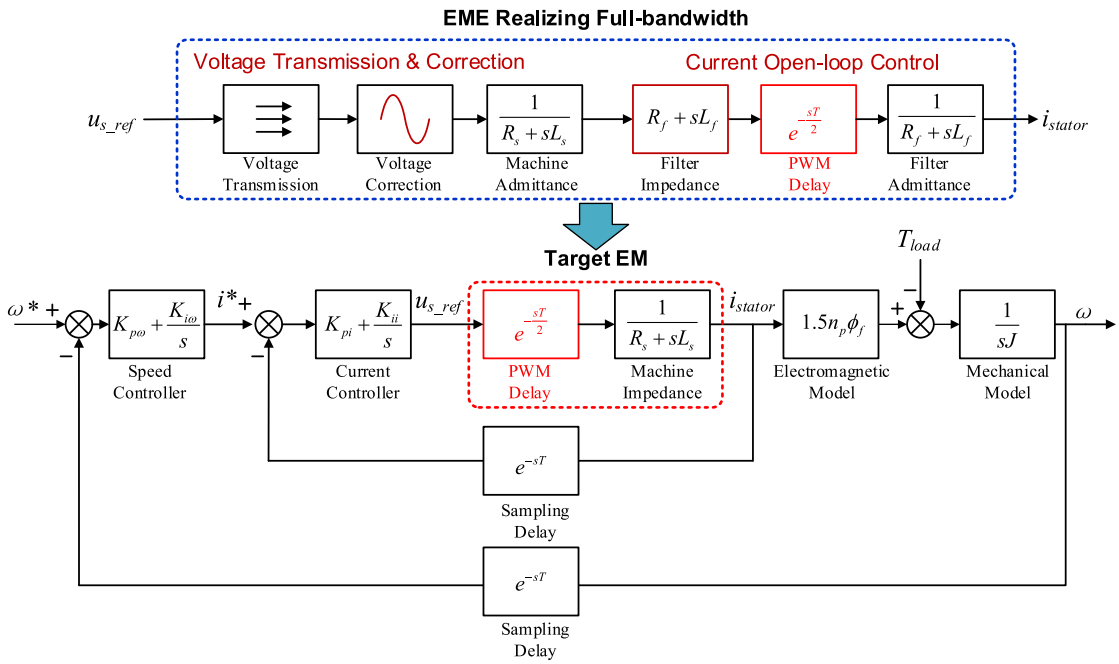

Fig. 7. Control diagram of EME realizing the full bandwidth.

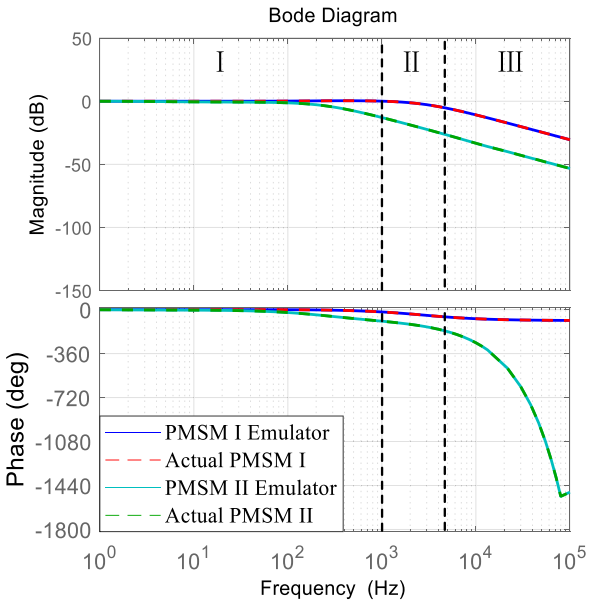

Fig. 8. Bode diagram of the current inner loop in FOC based on the EME realizing the full-bandwidth emulation and the actual PMSMs.

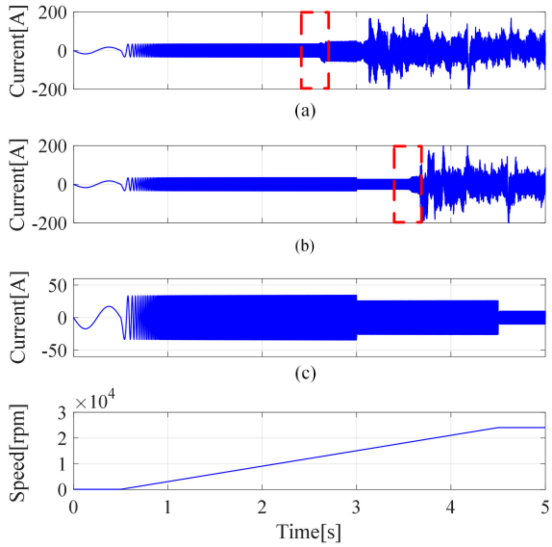

Fig. 9. Comparison in current response. (a) Typical method with CLCC and LPF for voltage sampling. (b) Typical method with CLCC and PWM voltage sampling. (c) Proposed method realizing full-bandwidth mission profile emulation.

1) The rotational reference speed is designed as aperiodic ramp changes, which range from positive ramp changes to negative ramp changes to cover a wide range of bandwidth. There cannot be any rotational reference speed mutation, or the drive system will go unstable.
2) The load mechanical torque is designed as aperiodic step changes, which can cover a full range of bandwidth in case of the electromagnetic torque characteristics as well as the current characteristics.

The mission profile for simulation analysis is defined as follows: the rotational speed is set as 60 r/min at first in order to simulate the soft start of the target electric machine. At 0.5 s, the electric machine is accelerated to 24 000 r/min, where the fundamental electrical frequency is set as 800 Hz at 4 s. The load torque is initially 2 N·m and steps to 1 N·m at 3 s.

In Fig. 9, the comparison in the current response of the typical EME and the proposed EME realizing the full-bandwidth emulation is illustrated. At around 2.5 s, the typical EME with the CLCC and the LPF for voltage sampling loses control, as

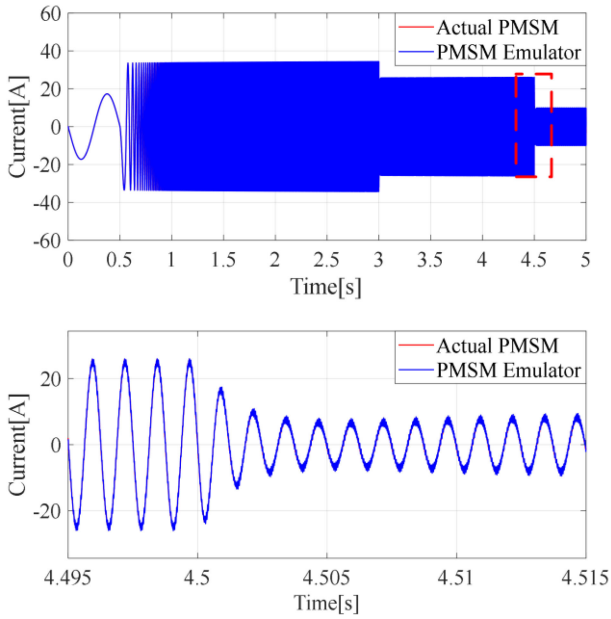

Fig. 10. Static and dynamic performance in current response of the EME realizing the full-bandwidth emulation.

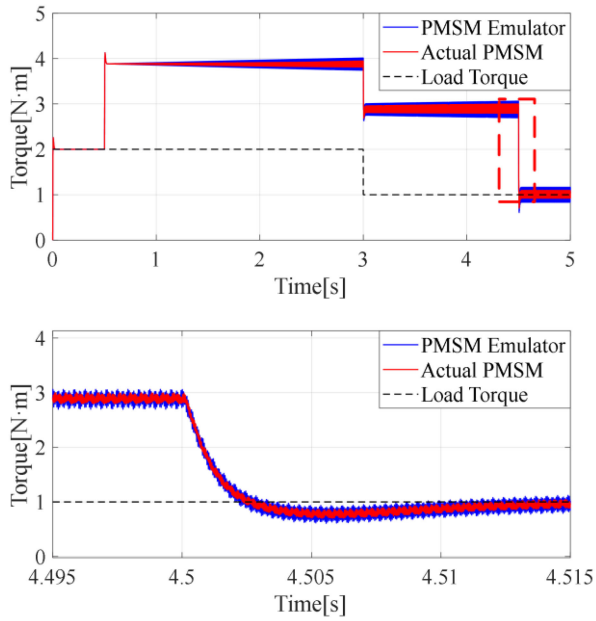

Fig. 11. Static and dynamic performance in torque response of the EME realizing the full-bandwidth emulation.

shown in Fig. 9(a), and the upper electrical frequency limitation is around 400 Hz, because the CLCC and LPF both limit the bandwidth of the emulation. At about 3.5 s, the typical EME with CLCC with the direct PWM voltage sampling loses the stability, as shown in Fig. 9(b), and the upper electrical frequency limitation is around 600 Hz. It indicates that getting rid of the LPF for voltage sampling enhances the bandwidth of emulation, but the CLCC is still the limiting factor. As shown in Fig. 9(c), the system based on the EME proposed, which realizes the full-bandwidth mission profile emulation can keep stable during the whole process.

Fig. 10 shows the static and dynamic performance in the current response of the EME realizing the full-bandwidth mission profile emulation. First, the system keeps stable and the current amplitude envelope is the same as the actual one. Second, at 4.5 s, when the current steps, it takes both the system based on the actual PMSM and the proposed EME about eight cycles to achieve the new steady state, and the current waveforms match well. The dynamic performance in the current response is correctly restored.

In Fig. 11, the static and dynamic performance in torque response of the EME realizing the full-bandwidth mission profile emulation is illustrated. Similar to the current response, the EME also achieves an outstanding static and dynamic performance in torque response under such high fundamental frequency.

B. Experimental Validation—Dynamic Performance in Load Transients and Steady State in High Frequency

The experimental setup is shown in Fig. 12, consisting of two major VSCs connected face-to-face. In the testing setup, the design for the drive-side converter and the emulating-side converter are the same. However, the configuration and design of the converters on the two positions may be different, this is a further research topic and is not discussed in this article. The topology of the experimental setup is the same as Figs. 1 and 4. The drive controller and emulating controller are implemented on individual TMS320F28335 DSPs. The parameters of the target emulating electric machine are listed in Table II. The experiment parameters are listed in Table III.

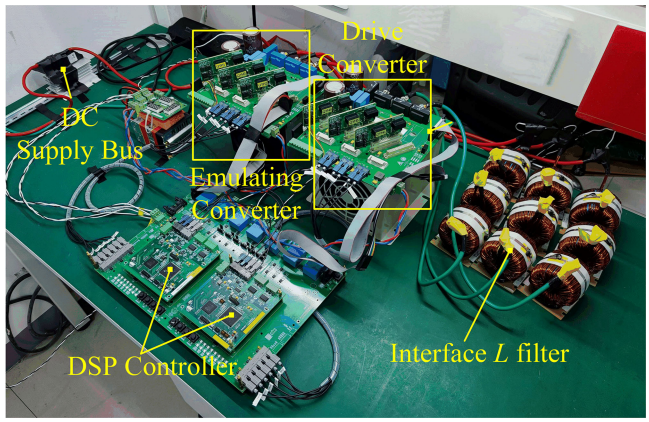

Fig. 12. Schematic diagram of the experimental setup.

TABLE III
PARAMETERS OF THE EXPERIMENTAL SETUP

Variable	Symbol	Value	Unit
DC Voltage Supply	V_{DC}	400	V
Switching Frequency	f_{sw}	20	kHz
Control Frequency	f_{ct}	20	kHz
Inductance of the L filter	L_f	1.38	mH
Resistance of the L filter	R_f	1.22	Ω

For certain limitations of the actual electric machine as experimental equipment, the further performance of the drive

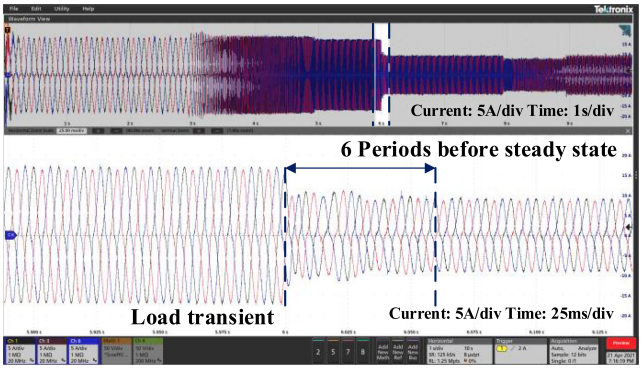

Fig. 13. Current dynamic response of the EME with the CLCC and the LPF for voltage sampling.

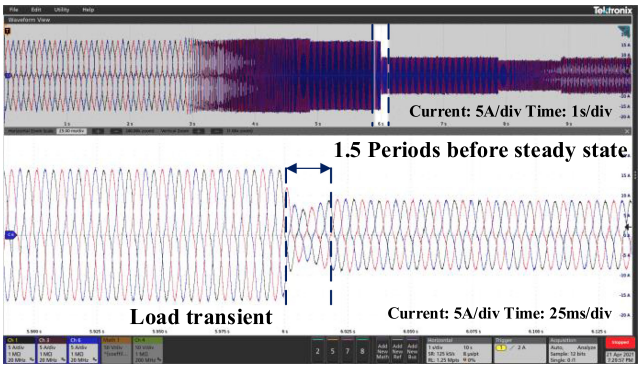

Fig. 14. Current dynamic response of the proposed EME with the OLCC and the voltage reference signal transmission.

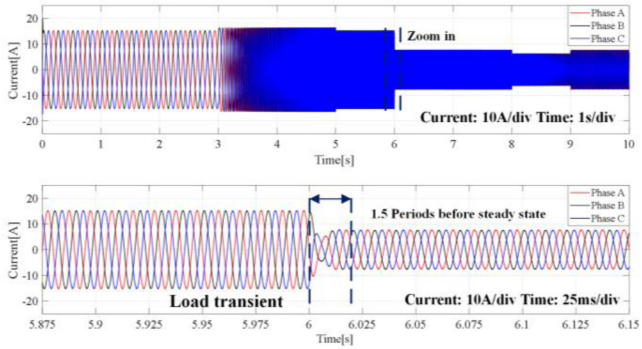

Fig. 15. Current dynamic response of the drive system based on the actual PMSM.

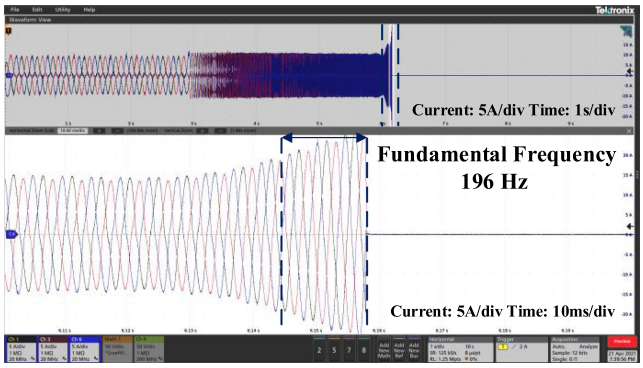

Fig. 16. Current static response of the typical EME with the CLCC and the LPF for voltage sampling.

system based on the actual electric machine is provided based on PLECS. The proposed EME realizing the full-bandwidth emulation mission profile can be verified according to the comparison between the provided experiment and simulation results.

Target electric machine parameters are listed in Table II, and the mission profile for dynamic performance comparison is given in the following.

The rotational speed is set as 60 r/min at first in order to simulate the soft start of the target electric machine. At 3 s, the electric machine is accelerated to 1500 r/min within 2 s, where the fundamental electrical frequency is 100 Hz. At 8 s, the speed is decelerated to 600 r/min within 1 s. The load torque is initially 2 N·m and steps to 1 N·m at 6 s.

The results of the dynamic performance comparison experiments between the typical EME and the proposed EME are shown in Figs. 13 and 14. Moreover, Fig. 15 gives the dynamic performance of the drive system based on the actual PMSM system in PLECS simulation, and the simulation is set to be the same as the experiment. The stator current is selected as the main focus, because the harmonics component of the stator current is little, and the dynamic performance of the stator current can easily reflect the performance of other key characteristics of the target electric machine according to (5), (9), and (10).

For the typical EME with an LPF for voltage sampling and CLCC, it takes about six fundamental periods to transit to the new current stable situation, and the transition process is drastic in terms of the amplitude of the current. However, for the EME realizing full-bandwidth emulation, it can be found that the settling time is much shorter (about one and a half fundamental period) and there are no significant oscillations on the amplitude of the current. Moreover, compared with the drive system based on the actual PMSM, the proposed EME realizing full-bandwidth emulation performs almost the same. Thus, the dynamic performance is greatly improved and the higher bandwidth can be guaranteed.

To compare the static performance under a relatively high frequency, another mission profile is given. The target electric machine is the same one in the dynamic performance experiment, and the mission profile is given in the following.

The rotational speed is set as 60 r/min at first in order to simulate the soft start of the target electric machine. At 3 s, the electric machine is accelerated to its rated highest speed (3900 r/min) within 4 s, where the fundamental electrical frequency is 260 Hz. The load torque is 1 N·m and has no step.

The results of the static performance comparison experiments under a relatively high frequency are shown in Figs. 16 and 17. Moreover, Fig. 18 gives the dynamic performance of the drive system based on the actual PMSM system in PLECS simulation, and the simulation is set to be the same as the experiment. The stator current is still selected as the main focus, and the stability

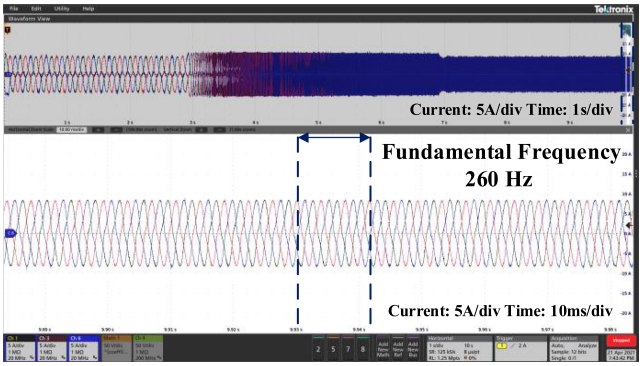

Fig. 17. Current static response of the proposed EME with the OLCC and the voltage reference signal transmission.

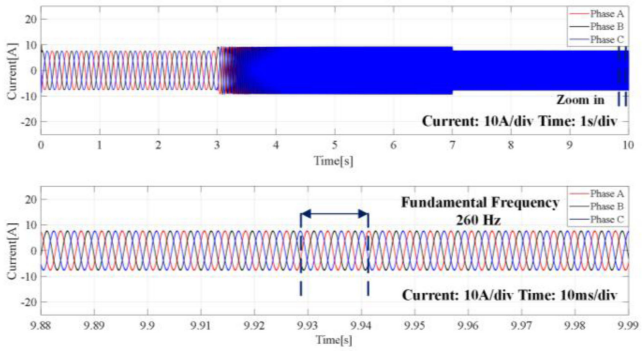

Fig. 18. Current static response of the drive system based on the actual PMSM.

of the current is to represent the static characteristics of the EMEs.

For the typical EME with an LPF for voltage sampling and CLCC, when the electrical frequency is accelerated to around 196 Hz, where the mechanical speed is around 2940 r/min, the drive system loses stability and the software protection in the drive side takes place, the experiment process has to be shut down. However, the drive system based on the proposed EME keeps stable during the whole mission profile, and operates well under the highest rated speed, where the electrical frequency is accelerated to around 260 Hz and the mechanical speed is around 3900 r/min. Moreover, compared with the drive system based on the actual PMSM, the proposed EME realizing full-bandwidth emulation performs almost the same. Thus, the static performance under high frequency can be greatly improved when the EME realizing full-bandwidth emulation is applied.

VI. Conclusion

In this article, an EME realizing the full-bandwidth mission profile is proposed. The proposed EME gets rid of the LPF for voltage sampling and CLCC, however, involves signal transport, voltage correction, and OLCC. The frequency-domain characteristic of the EME proposed in this article can be theoretically identical to that of the target machine. The proposed EME performs much better in the stability at high-frequency band according to the simulation validation as well as its dynamic performance according to the experimental validation. It can have much better performance in the test of the drive and control system applicable for the HSEM, and is expected to provide a more flexible and accurate emulation for increasingly complicated power electronics systems

Appendix

The parameters of the target PMSM studied in this article are shown in Tables I and II. The study cases are selected according to [29] and [30]. The parameters of the experimental setup are shown in Table III.

References

[1] K. Ma, M. Liserre, F. Blaabjerg, and T. Kerekes, "Thermal loading and lifetime estimation for power device considering mission profiles in wind power converter," *IEEE Trans. Power Electron.*, vol. 30, no. 2, pp. 590–602, Feb. 2015.

[2] K. Ma, U. Choi, and F. Blaabjerg, "Prediction and validation of wear-out reliability metrics for power semiconductor devices with mission profiles in motor drive application," *IEEE Trans. Power Electron.*, vol. 33, no. 11, pp. 9843–9853, Nov. 2018.

[3] K. Ma, J. Wang, X. Cai, and F. Blaabjerg, "AC grid emulations for advanced testing of grid-connected converters—An overview," *IEEE Trans. Power Electron.*, vol. 36, no. 2, pp. 1626–1645, Feb. 2021.

[4] K. Ma, H. Wang, and F. Blaabjerg, "New approaches to reliability assessment: Using physics-of-failure for prediction and design in power electronics systems," *IEEE Power Electron. Mag.*, vol. 3, no. 4, pp. 28–41, 2016.

[5] I. Vernica, K. Ma, and F. Blaabjerg, "Optimal derating strategy of power electronics converter for maximum wind energy production with lifetime information of power devices," *J. Emerg. Sel. Topics Power Electron.*, vol. 6, no. 1, pp. 267–276, 2018.

[6] K. Ma, N. He, M. Liserre, and F. Blaabjerg, "Frequency-domain thermal modelling and characterization of power semiconductor devices," *IEEE Trans. Power Electron.*, vol. 31, no. 10, pp. 7183–7193, 2016.

[7] J. Pippola, I. Vaalasranta, T. Marttila, J. Kiilunen, and L. Frisk, "Product level accelerated reliability testing of motor drives with input power interruptions," *IEEE Trans. Power Electron.*, vol. 30, no. 5, pp. 2614–2622, May 2015.

[8] H. J. Slater, D. J. Atkinson, and A. G. Jack, "Real-time emulation for power equipment development. II. The virtual machine," *Proc. Inst. Elect. Eng.—Elect. Power Appl.*, vol. 145, no. 3, pp. 153–158, May 1998.

[9] J. Wang, Y. Ma, L. Yang, L. M. Tolber, and F. Wang, "Power converter-based three-phase induction motor load emulator," in *Proc. 28th Annu. IEEE Appl. Power Electron. Conf. Expo.*, 2013, pp. 3270–3274.

[10] O. Vodyakho, M. Steurer, C. S. Edrington, and F. Fleming, "An induction machine emulator for high-power applications utilizing advanced simulation tools with graphical user interfaces," *IEEE Trans. Energy Convers.*, vol. 27, no. 1, pp. 160–172, Mar. 2012.

[11] Y. S. Rao and M. C. Chandorkar, "Real-time electrical load emulator using optimal feedback control technique," *IEEE Trans. Ind. Electron.*, vol. 57, no. 4, pp. 1217–1225, Apr. 2010.

[12] Q. Zhong and G. Weiss, "Synchronverters: Inverters that mimic synchronous generators," *IEEE Trans. Ind. Electron.*, vol. 58, no. 4, pp. 1259–1267, Apr. 2011.

[13] H. Wu *et al.*, "Small-signal modeling and parameters design for virtual synchronous generators," *IEEE Trans. Ind. Electron.*, vol. 63, no. 7, pp. 4292–4303, Jul. 2016.

[14] J. A. Suul, S. D'Arco, and G. Guidi, "Virtual synchronous machine-based control of a single-phase bi-directional battery charger for providing vehicle-to-grid services," *IEEE Trans. Ind. Appl.*, vol. 52, no. 4, pp. 3234–3244, Jul./Aug. 2016.

[15] K. S. Amitkumar, P. Pillay, and J. Bélanger, "An investigation of power-hardware-in-the-loop-based electric machine emulation for driving inverter open-circuit faults," *IEEE Trans. Transp. Electrific.*, vol. 7, no. 1, pp. 170–182, Mar. 2021.

[16] Y. R. Lee, Y. C. Kwon, and S. K. Sul, "DC-link voltage design of high bandwidth motor emulator for interior permanent-magnet synchronous motors," in *Proc. IEEE Energy Convers. Congr. Expo.*, 2018, pp. 4453–4459.

[17] Y. Luo, M. A. Awal, W. Yu, and I. Husain, "FPGA based high bandwidth motor emulator for interior permanent magnet machine utilizing SiC power converter," *IEEE J. Emerg. Sel. Topics Power Electron.*, vol. 9, no. 4, pp. 4340–4353, Apr. 2021.
[18] K. S. Amitkumar, R. S. Kaarthik, and P. Pillay, "A versatile power-hardware-in-the-loop-based emulator for rapid testing of transportation electric drives," *IEEE Trans. Transp. Electrific.*, vol. 4, no. 4, pp. 901–911, Dec. 2018.
[19] L. Bigarelli, M. di Benedetto, A. Lidozzi, L. Solero, and P. Grbovic, "FPGA-based permanent magnet synchronous machine emulator with sic power amplifier," *IEEE Trans. Ind. Appl.*, to be published, doi: 10.1109/TIA.2021.3104272.
[20] K. Ma and Y. Song, "Power-electronic-based electric machine emulator using direct impedance regulation," *IEEE Trans. Power Electron.*, vol. 35, no. 10, pp. 10673–010680, Oct. 2020.
[21] T. Roinila *et al.*, "Hardware-in-the-loop methods for real-time frequency response measurements of on-board power distribution systems," *IEEE Trans. Ind. Electron.*, vol. 66, no. 7, pp. 5769–5777, Jul. 2019.
[22] G. Si, J. Cordier, and R. M.Kennel, "Extending the power capability with dynamic performance of a power-hardware-in-the-loop application—Power grid emulator using 'inverter cumulation'," *IEEE Trans. Ind. Appl.*, vol. 52, no. 4, pp. 3193–3202, Jul./Aug. 2016.
[23] K. S. Amitkumar, R. Thike, and P. Pillay, "Linear amplifier-based power-hardware-in-the-loop emulation of a variable flux machine," *IEEE Trans. Ind. Appl.*, vol. 55, no. 5, pp. 4624–4632, Sep./Oct. 2019.
[24] P. C. Krause, O. Wasynczuk, and S. D. Sudhoff, *Analysis of Electric Machinery and Drive Systems*. Hoboken, NJ, USA: Wiley, 2002, pp. 191–206.
[25] I. Vernica, *Modelling and Implementation of Active Thermal Control Methods for Power Electronics Systems for Motor Drive Applications.* Aalborg, Denmark: Aalborg Univ. Press, 2016, pp. 7–16.
[26] R. Teodorescu, M. Liserre, and P. Rodríguez, *Grid Converters for Photovoltaic and Wind Power Systems*. Hoboken, NJ, USA: Wiley, 2011, pp. 207–209.
[27] N. R. Tavana and V. Dinavahi, "Real-time FPGA-based analytical space harmonic model of permanent magnet machines for hardware-in-the-loop simulation," *IEEE Trans. Magn.*, vol. 51, no. 8, pp. 1–9, Aug. 2015.
[28] S. Nandi, "A detailed model of induction machines with saturation extendable for fault analysis," *IEEE Trans. Ind. Appl.*, vol. 40, no. 5, pp. 1302–1309, Sep./Oct. 2004.
[29] Y. Liang, D. Liang, S. Jia, S. Chu, and J. He, "A full-speed range hybrid PWM strategy for high-speed permanent magnet synchronous machine considering mitigation of current harmonics," in *Proc. IEEE Energy Convers. Congr. Expo.*, Baltimore, MD, USA, 2019, pp. 1886–1890.
[30] L. Zhong, M. F. Rahman, W. Y. Hu, and K. W. Lim, "Analysis of direct torque control in permanent magnet synchronous motor drives," *IEEE Trans. Power Electron.*, vol. 12, no. 3, pp. 528–536, May 1997.

Yuhao Qi (Student Member, IEEE) received the B.Sc. degree in electrical engineering in 2020 from Shanghai Jiao Tong University, Shanghai, China, where he is currently working toward the M.Sc. degree in electrical engineering.

His research interests include the modeling, analysis, and control of motor drive systems, and mission profile emulation for motor drive systems.

Ke Ma (Senior Member, IEEE) received the B.Sc. and M.Sc. degrees in electrical engineering from Zhejiang University, Hangzhou, China, in 2007 and 2010, respectively, and the Ph.D. degree from Aalborg University, Aalborg, Denmark, in 2013.

He was an Assistant Professor with Aalborg University in 2014. In 2016, he joined the Faculty of Shanghai Jiao Tong University, China, as a tenure-track Research Professor, and is currently serving as the Deputy Director with the Key Laboratory of Control of Power Transmission and Conversion, Ministry of Education, China. His current research interests include the power electronics and its reliability in the application of renewable energy, HVDC, and motor drive systems. He is currently an Associate Editor for two IEEE Transaction journals, and Vice Chair for two IEEE Technical Committees. He was a recipient of "Excellent Young Wind Doctor Award 2014" by European Academy of Wind Energy, and several prized paper awards by IEEE.

Weiyu Tang received the B.Sc. and M.Sc. degrees in electrical engineering from Shanghai Jiao Tong University, Shanghai, China, in 2018 and 2021, respectively.

His research interests include the modeling, analysis and control of grid-tied converters, and filter design.